ELECTROCHEMISTRY

Prospects of halide-based all-solid-state batteries: From material design to practical application

Changhong Wang, Jianwen Liang, Jung Tae Kim, Xueliang Sun*

The safety of lithium-ion batteries has caused notable concerns about their widespread adoption in electric vehicles. A nascent but promising approach to enhancing battery safety is using solid-state electrolytes (SSEs) to develop all-solid-state batteries, which exhibit unrivaled safety and superior energy density. A new family of SSEs based on halogen chemistry has recently gained renewed interest because of their high ionic conductivity, high-voltage stability, good deformability, and cost-effective and scalable synthesis routes. Here, we provide a comprehensive review of halide SSEs concerning their crystal structures, ion transport kinetics, and viability for mass production. Furthermore, their moisture sensitivity and interfacial challenges are summarized with corresponding effective strategies. Last, halide-based all-solid-state Li-ion and Li-S pouch cells with energy density targets of 400 and 500 Wh kg^{-1} are projected to guide future endeavors. This work serves as a comprehensive guideline for developing halide SSEs from material design to practical application.

INTRODUCTION

Since their commercialization in 1991, lithium-ion batteries (LIBs) have played a pivotal role in enabling portable electronics, electric vehicles, and grid-scale energy storage. Still, LIBs continue to dominate the battery industry, powering millions of devices across the globe. However, with the rise of next-generation devices such as aerial drones and electric planes, there has been a surging demand for new battery technology that can surpass the fast-approaching physicochemical limit of current LIBs and address the safety concerns that arise from their highly flammable liquid electrolyte component. Thus, concerted efforts have been made to develop next-generation energy storage technologies with high energy density and intrinsic safety (*1*–*4*). In this context, all-solid-state batteries (ASSBs) have been revived to meet these criteria, beginning with the revisitation of various solid-state electrolytes (SSEs) based on different anion chemistries, including oxides (*5*–*7*), sulfides (*8*–*10*), borohydrides (*11*, *12*), and halides (*13*–*16*). Among them, halide SSEs are considered the best candidates for enabling ASSB technology because of several intrinsic chemical features of halogen anions compared to chalcogen counterparts (*16*, *17*). First, monovalent halogen anions forming as a framework have a weaker coulombic force with lithium ions than divalent sulfur or oxygen anions during ion migration. Thus, Li-ion transport kinetics in halide SSEs are quicker, corresponding to higher ionic conductivity. Second, the ionic radii of halogen anions (Cl^- = 167 pm, Br^- = 182 pm, and I^- = 202 pm) are relatively larger than oxide and sulfide anions (O^{2-} = 126 pm and S^{2-} = 170 pm), indicating that halide SSEs have longer ionic bond lengths than oxides and sulfides, from which high ion mobility and good deformability are expected. Third, halide anions (especially for F^- and Cl^-) have a higher electrochemical redox potential than oxide and sulfide anions, thus offering higher oxidative stability. Inspired by these intrinsic chemical features, halide SSEs have been pursued since the 1930s however failed to receive wide attention due to their low room temperature ionic conductivity (*18*–*23*).

In 2018, Asano *et al.* (*16*) revisited the halide SSEs Li_3YCl_6 and Li_3YBr_6, demonstrating high room temperature ionic conductivity (> 1 mS cm^{-1}), high voltage stability, excellent deformability, and desirable dry air stability. This groundbreaking work has sparked global research interest in halide SSEs (*13*–*16*, *18*–*21*, *24*–*30*). Until now, various halide SSEs have been synthesized, spanning from fluorides to iodines, such as Li_3AlF_6 (*31*, *32*), Li_3GaF_6 (*33*), Li_3InCl_6 (*24*, *25*), Li_3ScCl_6 (*34*), spinel $LiSc_{2/3}Cl_4$ (*35*), Li_3ErCl_6 (*36*), Li_3YCl_6 (*37*, *38*), Li_3HoCl_6 (*39*), Li_3YBr_6 (*40*–*42*), Li_3HoBr_6 (*43*), Li_3InBr_6 (*44*), Li_2ZrCl_6 (*45*), $Li_{3-x}M_{1-x}Zr_xCl_6$ (M = Y, Er, Yb, and Fe) (*29*, *45*–*49*), Li_3LaI_6 (*50*), and Li_3ErI_6 (*51*). In parallel, halide Na-ion counterparts have also been developed (*52*, *53*), some of which include Na_2ZrCl_6 (*54*), $Na_{3-x}Er_{1-x}Zr_xCl_6$ (*55*), and $Na_{3-x}Y_{1-x}Zr_xCl_6$ (*56*). Apart from the advances made at the material level, promising electrochemical performance based on halide SSEs has also been broadly reported (*57*), such as ultralong cycling stability (*15*), high areal capacity (*15*), and high-voltage operation (*47*). As the quest for a preeminent SSE continues, there is a vital need to review state-of-the-art halide SSEs from fundamental research to practical engineering design.

Here, we first discuss the structural characteristics of SSEs using halogen chemistry. The recent progress of halide SSEs is summarized in terms of their room temperature ionic conductivity, electrochemical window, material cost, and elemental abundance. Moreover, recent advances in understanding moisture stability are discussed. Halide-based ASSBs are presented with an emphasis on interfacial compatibility, particularly their cathode interface stability and anode interfacial challenges. Last, practical all-solid-state pouch cells (including NMC811/Li and Li-S) are numerically analyzed toward the energy density targets of 400 and 500 Wh kg^{-1}, respectively. This Review analyzes halide SSEs from fundamental materials synthesis to rational interface design to practical solid-state pouch cell engineering, intending to encourage more research toward developing practical ASSBs based on halide SSEs.

Structural category of halide SSEs

The search for new functional superionic conductors with a high room temperature ionic conductivity is an essential prerequisite for enabling high-performance ASSBs. In this regard, fundamental

Department of Mechanical and Materials Engineering, University of Western Ontario, London, ON N6A 5B9, Canada.
*Corresponding author. Email: xsun9@uwo.ca

guidelines based on well-known physicochemical parameters are highly desired to aid the design and discovery of new halide SSEs with high ionic conductivity. Here, we present the fundamental principles of the halogen anion framework and their effect on ion transport pathways.

Typically, the crystallographic structure of metal halide superionic conductors with a general formula of Li_3MX_6 (M = trivalent rare earth metal, X = F, Cl, Br, and I) is formed on the basis of the matrix LiX structure through M element dopping and vacancy formation. These structures hinge on the ionic radii of cations and anions, polarity, and ionic packing styles. On the basis of the law of ionic packing, the structure of halide SSEs is only stable when cations and anions are in close contact with each other. In other words, the radius ratio of cations to anions (r^+/r^-) must meet certain conditions (Fig. 1A) (*13*). According to this ionic packing law, most fluoride Li-ion conductors (F^-, 122 pm) tend to form a $LiMF_4$ phase with M ion occupancy in the cubic site of the F^- framework (MF_8 cube), as their radius ratio of M^{3+}/F^- is often greater than 0.732. Although fluoride SSEs have a wide electrochemical window, they generally exhibit a low ionic conductivity at room temperature (*31*), such as $LiAlF_4$ (1×10^{-6} S cm^{-1}) (*58*). Li *et al.* (*32*, *33*) synthesized Li_3AlF_6 and Li_3GaF_6 using ionic liquids, which exhibit a decent ionic conductivity close to 10^{-4} S cm^{-1} at room temperature. More efforts are required to understand the structure-to-performance relationship of fluoride SSEs. Compared with fluoride SSEs, chloride (Cl^-, 167 pm), bromide (Br^-, 182 pm), and iodide (I^-, 202 pm) superionic conductors tend to form a stable Li_3MX_6-type structure with the same local anion coordination environment of MX_6 octahedron, as their radius ratio, M^{3+}/X^-, is between 0.414 and 0.732 (*13*).

In terms of typical ternary halide SSEs with a general formula of Li_3MCl_6, there are two kinds of anion sublattice structures, which include hexagonal close packing (hcp) (Fig. 1B) and cubic close

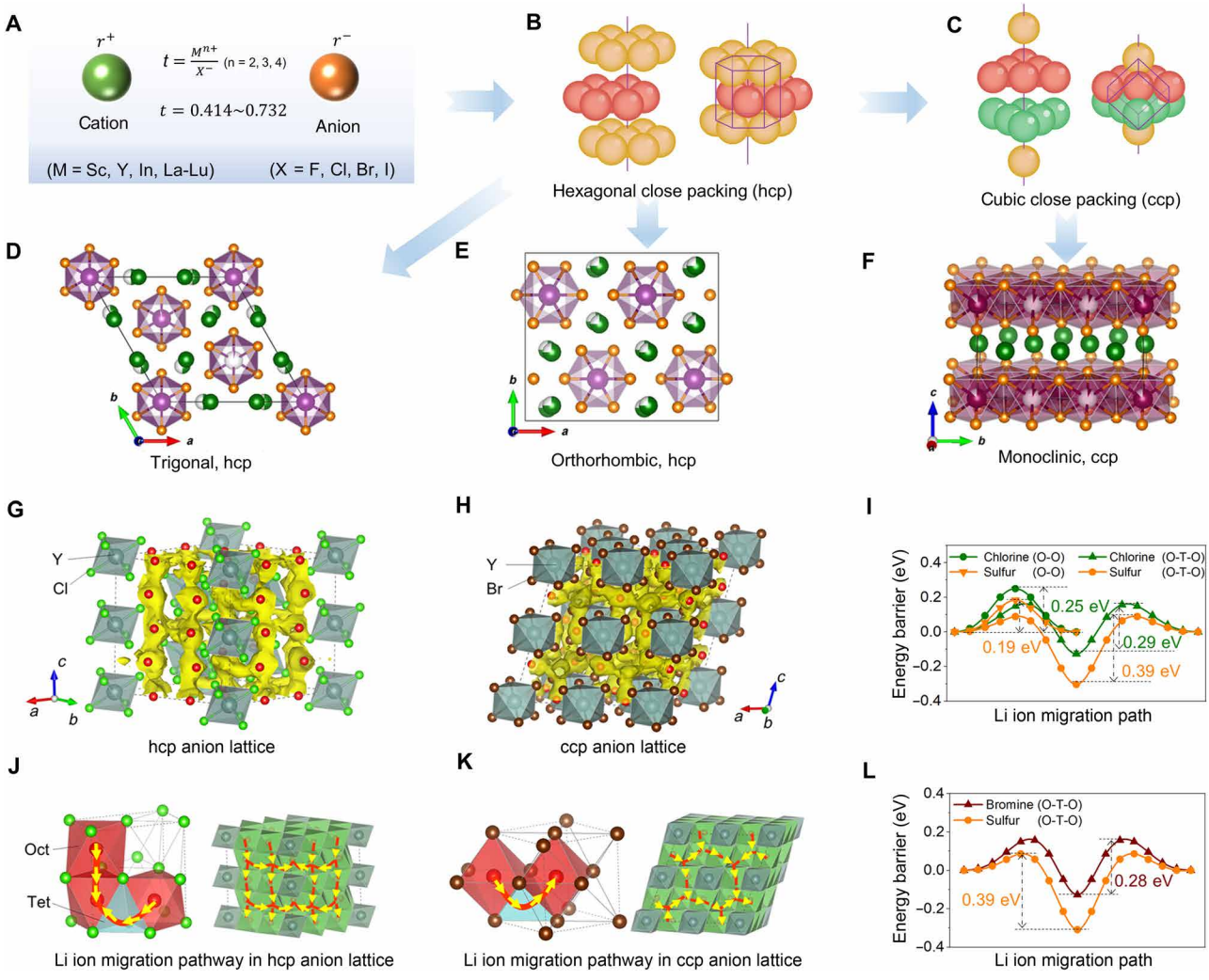

Fig. 1. Crystallography and ion transport kinetics of halide SSEs. (**A**) crystal radius ratio of cation to anion. (Cation: Li^+ = 90 pm, M^{3+} = 88 ~ 118 pm; F^- = 122 pm, Cl^- = 167 pm, Br^- = 181 pm, and I^- = 202 pm). The radius is from Shannon's research (*115*). (**B**) Hexagonal closest packing of halogen ions. (**C**) Cubic closest packing of halogen ions. (**D**) A trigonal crystal structure ($P\bar{3}m1$) with hcp anion arrangement. (**E**) An orthorhombic crystal structure (Pnma) with an hcp anion arrangement. (**F**) A monoclinic crystal structure (C2/m) with a ccp anion arrangement. Adapted with permission from (*79*). Copyright 2020, ACS (The American Chemical Society). (**G**) Crystal structures of Li_3YCl_6 with hcp-like anion lattice and (**H**) Li_3YBr_6 with ccp-like anion lattice, superimposed with Li^+ probability density marked by yellow isosurfaces from AIMD simulations. (**I**) The energy landscape of single Li-ion migration in hcp sublattice. (**J**) The Li-ion migration pathways in Li_3YCl_6. (**K**) The Li-ion migration pathways in Li_3YBr_6. (**L**) The energy landscape of single Li^+ migration in ccp sublattice. Adapted with permission from (*17*). Copyright 2019, Wiley.

packing (ccp) (Fig. 1C). The average ionic radius of metal cations plays a decisive role in the crystal structure, which can be further divided into three space groups. The first is a trigonal structure ($P\bar{3}m1$) with an hcp anion sublattice (hcp-T), in which M^{3+} cations with a relatively larger ionic radius ranging from 106.4 to 102 pm (e.g., Tb^{3+} = 106.3 pm, Dy^{3+} = 103 pm, Ho^{3+} = 104.1 pm, and Er and Tm = 102 pm) normally occupy its octahedral sites (Fig. 1D). The second is an orthorhombic structure (Pnma) with an hcp anion sublattice (hcp-O), their octahedral sites are usually taken by M^{3+} cations with a relatively small ionic radius spanning from 102 to 100 pm (e.g., Yb^{3+} = 100.8 pm and Lu^{3+} = 100.1 pm) (Fig. 1E). The third is a monoclinic structure with an ABCABC stacking of the ccp anion sublattice (ccp-M) (Fig. 1F), in which the octahedral sites are occupied with M^{3+} cations with an ionic radius less than 100 pm (e.g., In^{3+} = 94 pm and Sc^{3+} = 88.5 pm). The representative halide SSEs are $Li_2Sc_{2/3}Cl_4$ (space group of $Fd\bar{3}m$) and monoclinic Li_3InCl_6 (space group of C2/m). Unlike ternary chlorides, all the ternary bromides and iodides of Li_3MBr_6 and Li_3MI_6 fall into the ccp-M structure and theoretically should exhibit high ionic conductivities. However, only a few bromides and iodides with high ionic conductivities have been reported thus far. It can be inferred that many potential components with high ionic conductivity can be discovered because of their structural characteristics.

Li transport kinetics in halide SSEs are also closely related to their anion framework (*36*, *50*, *59*–*61*). Different anion sublattices lead to different ion transport pathways. In an hcp anion sublattice (e.g., Li_3YCl_6; Fig. 1G), ion diffusion is anisotropic with fast *c*-axis one-dimensional (1D) diffusion channels, where Li-ions hop among adjacent face-sharing octahedral sites (Fig. 1J). These 1D *c* channels are connected through the *ab* planes through tetrahedral (Tet) interstitial sites, forming an anisotropic 3D diffusion network. In the ccp anion sublattice, e.g., Li_3YBr_6, Li^+ diffusion occurs through a 3D isotropic network, where Li^+ ions hop to the other octahedral sites through Tet sites (Fig. 1K). Whether the anion framework exhibits an hcp or ccp structure, the energy barrier for single Li^+ migration in halide SSEs is still considerably lower than sulfide anions in both cases (Fig. 1, I and L), indicating the great potential to obtain high ionic conductivity based on halogen chemistry (*16*).

Besides the ion-migration pathway, Li content and the cation sublattice have a profound influence on factors such as low cation concentration and sparse cation distribution, which play a critical role in determining the overall ionic conductivity, as demonstrated by Mo's group via first-principles calculations (*59*). On the basis of these findings, they concluded the following: (i) low Li content, typically between 40 and 60% of the available octahedron sites; (ii) low cation concentration; and (iii) sparse cation distribution are the three critical factors for improving ionic conductivity of halide SSEs. Moreover, tuning the defects and disordering of the sublattice is also a promising strategy to improve the ionic conductivity of halide SSEs further, which will be further discussed in the following section. Furthermore, new ion transport mechanisms, such as the anion rotation effect and multi-ion concerted migration, also need to be explored in the halogen anion framework (*62*–*64*).

Current advances and cost-effectiveness of halide SSEs

Along with theoretical advancements, many halide SSEs with decent ionic conductivity at ambient temperature have been experimentally synthesized. The most common way to summarize this progress is by the chemical elemental composition of A_3MX_6. Halide Na-ion conductors can be obtained by changing mobile ions from Li-ion to Na-ion at the A site (*53*). Changing trivalent metal cations at the M site leads to halide SSEs with different reduction potentials (*17*, *65*). Altering halogen anions at the X site can adjust the oxidation stability of halide SSEs ($F^- > Cl^- > Br^- > I^-$) (*66*). To better understand the structure-to-performance relationship, we summarize the ionic conductivity of various halide SSEs according to their anion sublattice and space groups (Fig. 2A). It can be seen that monoclinic halide SSEs with a ccp anion sublattice demonstrate much higher ionic conductivity than trigonal and orthorhombic halide SSEs with an hcp framework. The general trend of ionic conductivity is $\sigma_{monoclinic} > \sigma_{orthorhombic} > \sigma_{trigonal}$ (*48*).

On the basis of the ccp anion sublattice, many monoclinic halide SSEs have demonstrated decent ionic conductivity at room temperature. For instance, our group synthesized monoclinic Li_3InCl_6 using a water-mediated synthesis route, exhibiting an ionic conductivity of 2.02 mS cm^{-1} (*24*). Recently, we reported monoclinic Li_3ScCl_6 with high ionic conductivity of 3 mS cm^{-1}, which was realized by tuning Li and Sc site occupations. The ionic conductivity that we reported is based on cold pressing. However, the ionic conductivity can be further enhanced by minimizing grain boundary resistance using hot pressing. This has been verified by Chen's group, demonstrating that the ionic conductivity of $Li_3Y(Br_3Cl_3)$ can reach 7.2 mS cm^{-1} after hot pressing (*26*). It should be noted that the ionic conductivity of SSEs tested by different methods and under different conditions (i.e., pressure and processing atmosphere) has some variations (*67*).

On the basis of the hcp anion sublattice, trigonal and orthorhombic halide SSEs usually present a relatively lower ionic conductivity (*15*, *24*, *25*, *34*, *43*). However, many promising strategies have been proposed to enhance their ionic conductivity, including: (i) aliovalent substation; (ii) tuning cation site disorder; (iii) introducing microstrain; and (iv) stacking faults. Aliovalent substitution is the most common strategy to enhance the ionic conductivity of halide SSEs with an hcp sublattice, which boosts the ionic conductivity over 1 mS cm^{-1} (Fig. 2B) (*29*, *45*, *46*, *48*). The trigonal and orthorhombic structure changes to a new orthorhombic structure (orthorhombic-II) by aliovalent substitution (e.g., Zr, Hf, and Fe) (*46*, *47*). Zeier's group proposed that the ionic conductivity of Li_3YCl_6 can reach 1 mS cm^{-1} by increasing the disorder of Y2 and Y3 sites in the *z*-direction through a mechanochemical synthesis process (*68*). Moreover, a microstrain induced by an ammonium-assisted wet chemistry synthesis process is found to be beneficial to Li-ion transport, particularly for halide SSEs with an hcp anion sublattice (e.g., Li_3YCl_6 and Li_3ErCl_6) (*69*). Recently, Sebti *et al.* (*70*) revealed the presence of a high concentration of stacking faults in Li_3YCl_6 through a mechanochemical synthesis process. These stacking faults and Li defect layers generate additional site linkages with lower migration barriers and facilitate Li-ion transport. All the previous results demonstrate that structural tuning can substantially influence the ionic conductivity of halide SSEs (*68*, *71*, *72*). On the basis of our understanding, halide SSEs with an hcp anion sublattice have an anisotropic ion transport network, in which ion transport in the *z*-direction is likely the rate-determining step (*39*). Therefore, any strategy facilitating ion transport along the *z*-direction can increase the ionic conductivity of halide SSEs.

In terms of the voltage stability of halide SSEs, fluoride-based ones demonstrate the widest electrochemical window, indicating their high oxidation stability and low reduction stability (Fig. 2C).

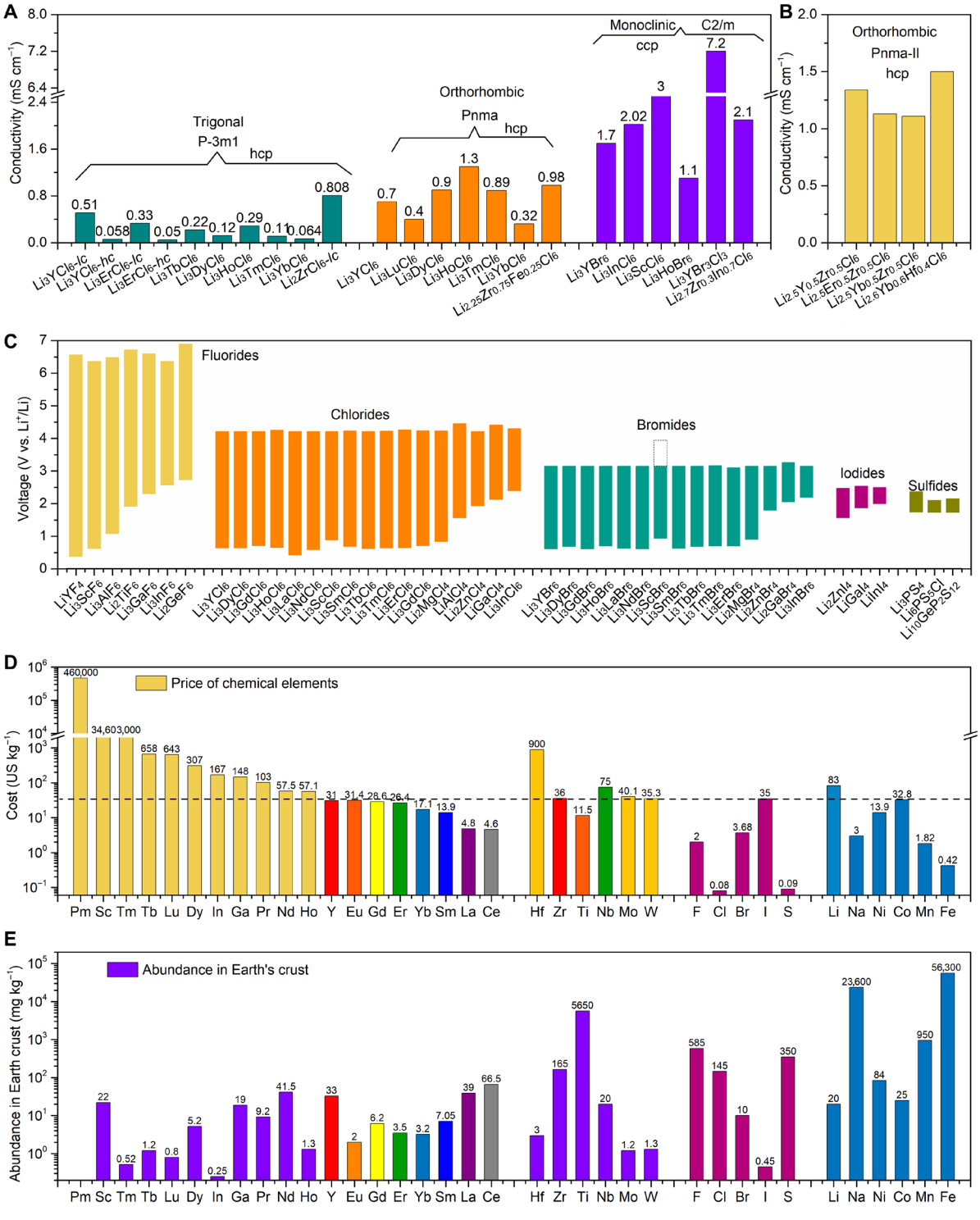

Fig. 2. Ionic conductivity, electrochemical window, cost, and abundance of halide SSEs. (**A** and **B**) Room temperature ionic conductivity of ternary halide electrolytes and quaternary halide electrolytes. (**C**) The electrochemical window of halide SSEs in comparison with sulfides. The data are reproduced with permission from (*17*). Copyright 2019, Wiley. (**D** and **E**) Price of chemical elements used for halide SSEs and their abundance in Earth's crust. The data are obtained from "prices of chemical elements" on Wikipedia.

However, fluoride-based halide SSEs exhibit low ionic conductivities, which originates from their structural characteristics. The low ionic conductivity of fluoride SSEs considerably constrains their practical application for ASSBs. Chloride-based halide SSEs also demonstrate high voltage stability (>4 V), while most bromides show lower oxidization stability of approximately 3.2 V, other than Li_3ScBr_6, which shows high voltage stability based on theoretical calculations (*17*). Iodine has an electrochemical window comparable to sulfide SSEs. Considering their electrochemical window, fluoride and chloride SSEs are suitable choices for high-voltage transition metal oxides. Conversely, bromide and iodide SSEs are good choices for developing solid-state lithium-sulfur (Li-S) and lithium-oxygen (Li-O_2) batteries considering that the operating voltage of these battery systems falls between their electrochemical windows (*43*, *73*). Several essential points should be mentioned regarding the electrochemical window of halide SSEs. First, when determining the electrochemical stability of halide SSEs using cyclic voltammetry, the initial potential should be used to determine the electrochemical window rather than the peak voltage. Second, using carbon additives to provide sufficient electron conduction pathways is essential for obtaining intrinsic electrochemical stability (*74*).

Halide SSEs have satisfied many criteria required for application in ASSBs, such as high ionic conductivity and high-voltage stability. However, the practicality of halide SSEs is still under question, as they are often composed of costly metallic elements. Thus, it is crucial to analyze the cost of halide SSE materials. Figure 2 (D and E) summarizes the average price and abundance of different chemical elements typically used for halide SSEs, using cobalt as a reference. Most trivalent metals are far more expensive than cobalt, except for a few, such as Y, Eu, Gd, Er, Yb, Sm, La, and Ce. Although the latter is cheaper than cobalt, they are not abundant in Earth's crust. In this regard, elements such as Y, La, Ce, Zr, Ti, and Nb are more practical. Although many halide SSEs are composed of expensive metals, this can be alleviated by aliovalent substitution with cheap metals, thus reducing their cost and increasing their ionic conductivity, as demonstrated in recent works (*45*–*47*, *75*). In addition, the price generally goes down when worldwide production increases.

Moisture stability of halide SSEs

Another concern for deploying halide SSEs in ASSBs is their moisture sensitivity (*76*). In general, most halides are hygroscopic and easily absorb water molecules from the surrounding environment (Fig. 3A). This property is also known as deliquescence. To address this challenge, Zhu *et al.* (*76*) conducted a systematic thermodynamic analysis for a wide range of ternary halide materials, which provides a theoretical guideline for designing air-stable halide SSEs. Their theoretical analyses confirm that In^{3+} cation shows the best moisture stability, which is in good agreement with the experimental results (*25*). Figure 3B shows a guiding chart for cation selection to simultaneously achieve good moisture and reduction stability (toward the top right corner), paving the way for the development of air-stable SSEs based on chloride chemistry.

Experimentally, Li *et al.* (*77*) investigated the air stability of Li_3InCl_6 and Li_3YCl_6 and their degradation mechanism upon exposure to air. In comparison, the water absorption rate of Li_3InCl_6 is quicker than that of Li_3YCl_6, whereas the amount of water absorption of Li_3YCl_6 is more than that of Li_3InCl_6 due to the higher solubility of $InCl_3$ compared to YCl_3. The air stability is closely related to the contact area of the halide SSEs with air (Fig. 3C). Our group also used in situ and operando synchrotron x-ray analytical techniques to probe the degradation mechanism of Li_3InCl_6 upon exposure to air (*78*). We found that a portion of Li_3InCl_6 reacts with H_2O to form In_2O_3, LiCl, and HCl, while the remaining Li_3InCl_6 absorbs moisture to form the hydrate $Li_3InCl_6{\cdot}xH_2O$. In dry room conditions with a dew point of −40°C, the ionic conductivity decay of Li_3InCl_6 upon exposure to air with a low humidity degree (3 to 5%) was slow, which indicated that Li_3InCl_6 can be easily integrated into ASSBs manufacturing in a dry room with a low dew point (*78*).

Several effective strategies have been proposed to ameliorate the poor air stability of halide SSEs, such as surface coatings and structural tuning. For example, atomic layer deposition techniques have been developed to coat a thin layer of Al_2O_3 on Li_3InCl_6 (Fig. 3D), effectively blocking their exposure to air and notably slowing down their degradation in ambient environmental conditions (Fig. 3E). Our group investigated the function of the M atom in Li_3MX_6 by tuning a series of $Li_3Y_{1-x}In_xCl_6$ ($0 \leq x < 1$) (*79*). When the ratio of In^{3+} was increased, a gradual structural conversion from the hcp anion arrangement to the ccp anion arrangement occurred (Fig. 3F). The humidity tolerance of $Li_3Y_{1-x}In_xCl_6$ is considerably enhanced when the In^{3+} content is high enough due to the formation of hydrated intermediates. As a result, the high ionic conductivity of $Li_3Y_{1-x}In_xCl_6$ is retained after exposure to humid air (Fig. 3G). Besides ALD (atomic layer deposition) coatings and structural tuning, developing intrinsically air-stable halide SSEs is also a good direction. For example, Ma *et al.* (*75*) recently reported a cost-effective Li_2ZrCl_6 with relatively high ionic conductivity and excellent air stability. Along with the strategies mentioned above, more efforts are needed to improve the air stability of halide SSEs, particularly new strategies from the viewpoint of the electronic structure.

Synthesis methods of halide SSEs

For the large-scale application of halide SSEs, cost-effective, green, and high-throughput production is critical. Now, three synthesis routes have been proposed, including mechanochemical synthesis (*68*), comelting (*34*, *80*), and wet-chemistry synthesis (*24*, *69*). Mechanochemical synthesis (e.g., high-energy ball milling) is considered a feasible method for halide SSE production (Fig. 4A). This method can obtain amorphous or low-crystallinity (or metastable) halide SSEs with narrow particle size distribution. In addition, the low crystallinity can be further enhanced by a post-annealing process. The comelting method is also a facile approach, in which two precursors are directly sealed in an ampoule tube and heated to form a solid solution based on a phase diagram (Fig. 4B). This method is beneficial for obtaining large crystalline sizes by carefully controlling the temperature and time (*81*). Wet chemistry was first reported by our group (Fig. 4C), which was successfully developed to synthesize Li_3InCl_6 (*24*). Recently, an ammonia-coordinate route was also proposed to synthesize various halide SSEs (*69*). In addition, a vacuum evaporation–assisted synthesis method was developed for the gram-scale synthesis of halide SSEs. The as-prepared Li_3HoBr_6 shows a decent ion conductivity close to the mS cm^{-1} level (*82*). Because of the viability of wet-chemistry synthesis, now kilogram-scale Li_3InCl_6 can be produced for large-scale application. Despite this, concerted efforts to develop scalable and cost-effective synthesis routes for the mass production of halide SSEs are still encouraged.

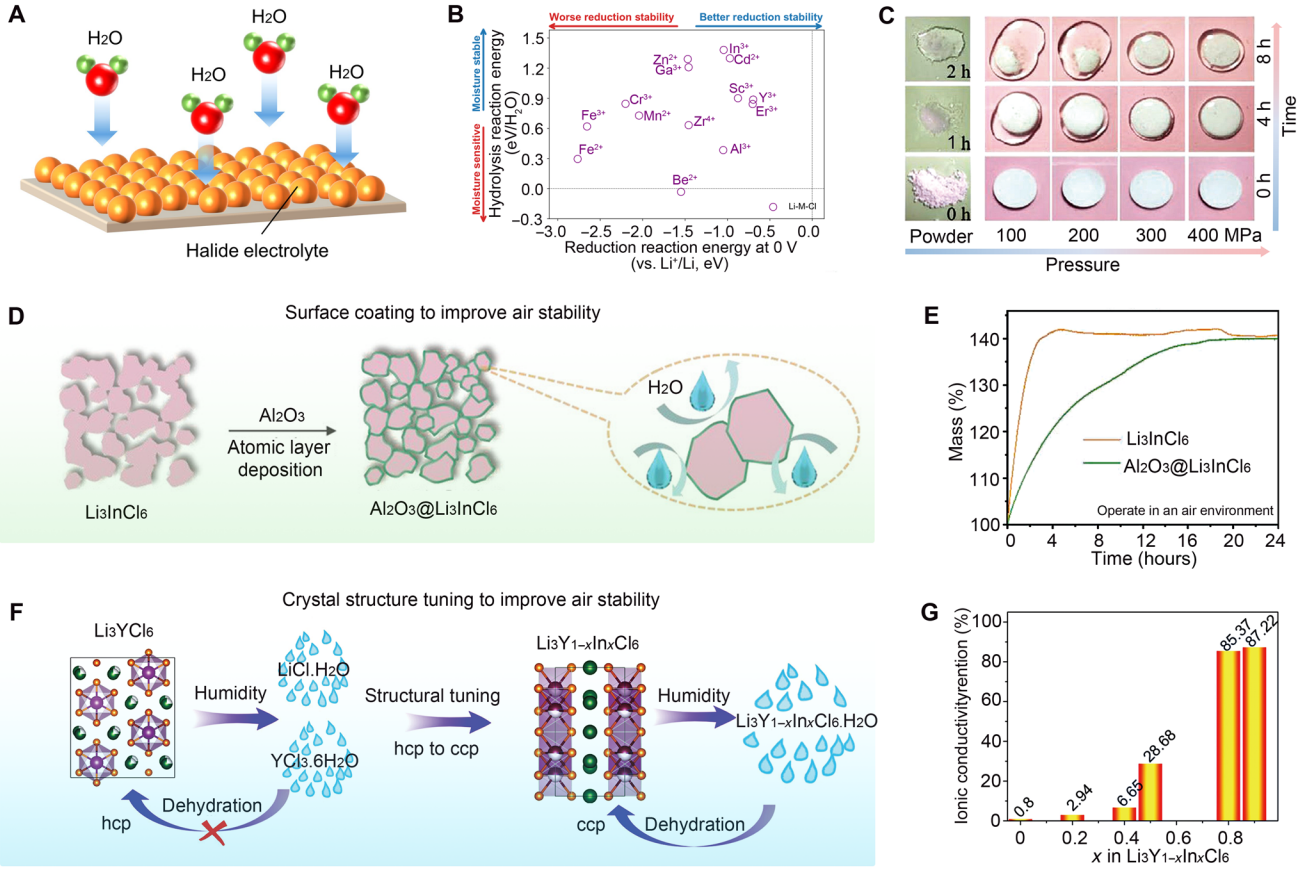

Fig. 3. Air stability of halide SSEs. (**A**) A schematic of a halide SSE absorbing water in the atmospheric environment. (**B**) The moisture stability versus reduction stability of 14 ternary lithium chlorides. Adapted with permission from (*76*), Copyright 2020, Wiley. (**C**) Halide SSEs with different exposure areas have different liquification rates. Adapted with permission from (*77*), Copyright 2021, Wiley. (**D**) Using a surface coating to mitigate the degradation of halide SSEs in air. (**E**) Pristine Li_3InCl_6 and Al_2O_3@Li_3InCl_6 powder shows different absorption rates. Adapted with permission from (*77*), Copyright 2021, Wiley. (**F**) Tuning crystal structure to alleviate the air instability of halide SSEs. (**G**) Ionic conduction retention of $Li_3Y_{1-x}In_xCl_6$ on the function of *x*. Adapted with permission from (*79*). Copyright 2020, ACS.

Fig. 4. Synthesis methods of halide SSEs. (**A**) High-energy ball milling. (**B**) Comelting. (**C**) Wet-chemistry synthesis.

The synthesis method also subtantially influences the ionic conductivity of halide SSEs. For instance, Zeier's group investigated the influence of the synthetic procedure on the structure and ionic transport properties of Li_3ErCl_6 and Li_3YCl_6. It is found that a cation defect within the structure in which Er/Y is disordered to a new position enormously benefits the transport properties (*68*). This work shows that the synthetic procedure can considerably affect the crystal structure and resulting diffusion pathways in superionic conductors.

Interfaces of halide ASSBs

Benefiting from their high-voltage stability, halide SSEs can directly contact high-voltage transition metal oxide cathodes (i.e., $LiCoO_2$ and $LiNi_{0.8}Mn_{0.1}Co_{0.1}O_2$) without any extra surface coatings. As demonstrated by Asano *et al.* (*16*), the initial charge and discharge curves of Li_3YCl_6@$LiCoO_2$/Li_3YCl_6/In-Li cells almost follow the $LiCoO_2$ electromotive force curve, indicating that minimal side reactions occur in this battery configuration. The initial coulombic efficiency is as high as 94.8% (Fig. 5A1). Such a high coulombic efficiency indicates that Li_3YCl_6 is highly stable against 4 V class

cathode active materials. Revealed by electrochemical impedance spectroscopy, the interfacial resistance between LYC and LCO is as low as 16. 8 ohm·cm^2, which is much smaller than 128.4 ohm·cm^2 for sulfide ASSBs (Fig. 5A2) (*16*). $LiCoO_2$-based ASSBs have high capacity retention of 98% at the 100th cycle. In addition, $LiNi_{0.6}Mn_{0.6}Co_{0.2}O_2$ and $LiNi_{0.8}Mn_{0.1}Co_{0.1}O_2$ have also demonstrated ultrastable cycling performance when using a halide SSE (*24*, *35*). Recently, Nazar's group demonstrated stable cycling over 3000 cycles with a capacity retention of 80% and a high areal capacity of 4 mAh cm^{-2} for 500 cycles (*15*), which almost meets the practical criteria. Despite this, the temperature-dependent electrochemical performance of halide-based ASSBs has not been thoroughly investigated yet, which is crucial for the all-weather application of EVs. In addition, some high-voltage cathodes, such as $LiCoPO_4$ (~4.8 V versus Li^+/Li) (*83*) and $LiNi_{0.5}Mn_{1.5}O_2$ (~4.7 V versus Li^+/Li) (*84*), have not been reported with halide SSEs. Although their high operation voltage is beyond the electrochemical windows of solid-state halide electrolytes, stabilizing their interface with solid-state halide electrolytes via advanced interface engineering is of particular interest.

Unlike the cathode interface, halide SSEs are relatively stable under elevated voltages due to the high oxidation potential of chloride anions. However, the central trivalent metal cations are not beneficial for their reduction potential. Therefore, halide SSEs are generally unstable at the anode interface, particularly when in contact with lithium metal anodes (*17*, *85*, *86*). As predicted by the density functional theory, direct contact with Li metal leads to considerable interfacial reactions and results in SSE degradation (*17*, *43*)

$$Li_3MX_6 + 3Li = 6LiCl + M\ (M = In., Y, etc.)$$

The most common strategy to alleviate this issue is to put a buffer layer between the halide SSE and Li metal. By exploiting the self-limiting reactions between Li_6PS_5Cl and Li metal, the ion/electron mixing interface between halide SSEs and Li metal can be converted into an ion-conducting interface, thus preventing halide SSE degradation (*37*, *69*). Therefore, using bilayer solid electrolytes (halide + sulfide) can enable the Li metal anodes in halide ASSBs. Janek *et al.* (*85*) recently

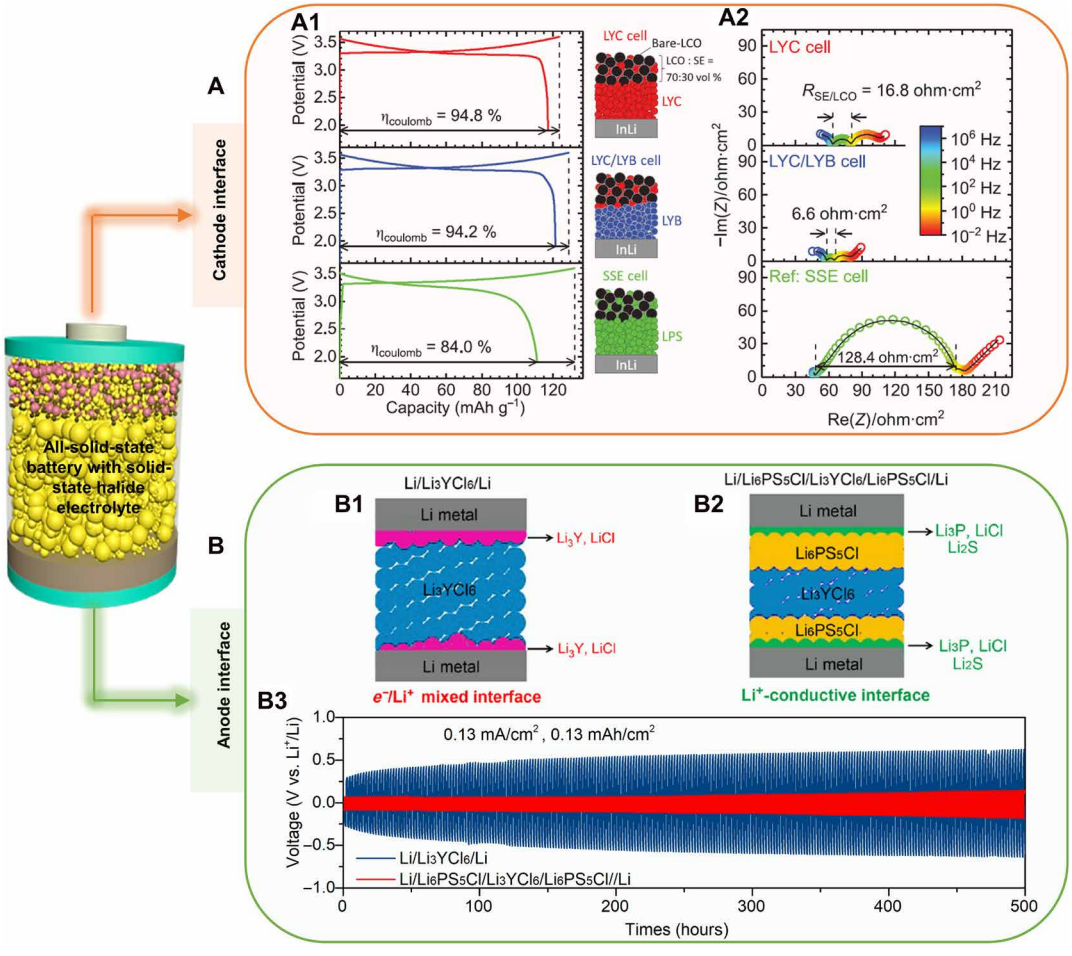

Fig. 5. Interface property of all-solid-state LIBs with halide SSEs. (**A**) **Cathode interface stability.** (A1) Initial charge/discharge curves of bulk-type ASSB cells at 25°C at 0.1 C. The schematic cell structures are drawn on the right side of each plot. (A2) The Nyquist plots of the electrochemical impedance spectroscopy spectra of ASSB cells after the first charging cycle. Open circles are the measured plot color-coded with the frequency. Black lines are the fitted curve using the equivalent circuit model. Adapted with permission from (*16*). Copyright 2018, Wiley. (**B**) Anode interface stability. (B1) The mixed electronic and ionic interface between lithium metal and Li_3YCl_6. (B2) The Li^+-conductive interface between Li_3YCl_6 and Li is enabled by a thin layer of Li_6PS_5Cl. (B3) The symmetric cell performance comparison. Adapted with permission from (*69*). Copyright 2021, AAAS.

demonstrated that the interfacial ion transport resistance between sulfide and halide SSEs is negligible. In contrary, Tarascon *et al.* (*87*) reported that halides are incompatible with sulfide SSEs (e.g., Li_6PS_5Cl and β-Li_3PS_4). More detailed studies are still required to understand the heterointerface between halide and sulfide SSEs. Counterintuitively, Yao *et al.* (*88*) recently reported Li-stable Li_2ZrCl_6 and Li_2HfCl_6. They claimed that the thick LiCl film formed between Li_2ZrCl_6 and Li, Li/Li_2ZrCl_6/Li symmetric cells demonstrated superior stability against Li metal anodes with 4000 hours of steady lithium plating/stripping at 0.1 mA cm^{-2}. However, soft breakdown frequently occurs in solid-state Li symmetric cells, resulting in misleading Li stability. A rigorous examination of solid-state Li/SSE/Li symmetric cells is strongly recommended to exclude the soft breakdown in the future (*89*).

Other than sulfide SSEs, some Li-stable SSEs, such as nitrides (*90*), borohydrides (*91*, *92*), and antiperovskites (*93*, *94*), are also excellent choices for stabilizing Li metal anode in halide ASSBs. Besides, some organic solid polymer electrolytes and inorganic-polymer composites that are compatible with Li metal and halide SSEs are also worth developing for halide ASSBs (*4*, *95*, *96*). Besides Li metal, other anode materials, such as silicon (*97*), silicon-carbon composites (*98*), and $Li_4Ti_5O_{12}$ (*10*) and alloy anodes (*99*–*101*), are also worth investigating in halide ASSBs considering their high thermal stability and low-cost fast-charging capability. Using halide SSEs to develop anode-free ASSBs will also be an emerging direction for realizing ultrahigh energy density (*2*).

Halide SSEs for all-solid-state Li-S/Li-Se/Na-ion batteries

Apart from their application in all-solid-state LIBs, halide SSEs have also been used in other electrochemical energy storage systems (Fig. 6A), such as all-solid-state Li-S batteries (*43*), all-solid-state Li-Se batteries (*102*), solid-state Li-O_2 batteries (*73*), and all-solid-state Na-ion batteries (*56*). Compared with all-solid-state LIBs, Li-S chemistry offers higher energy density (2600 Wh kg^{-1}), better cost-effectiveness, and compatibility with halide SSEs. Moreover, all-solid-state Li-S chemistry is free of the notorious "polysulfide shuttle" phenomenon (*103*, *104*). Recently, Du *et al.* (*43*) synthesized Li_3HoBr_6 with a decent ionic conductivity of 1.1 mS cm^{-1} at room

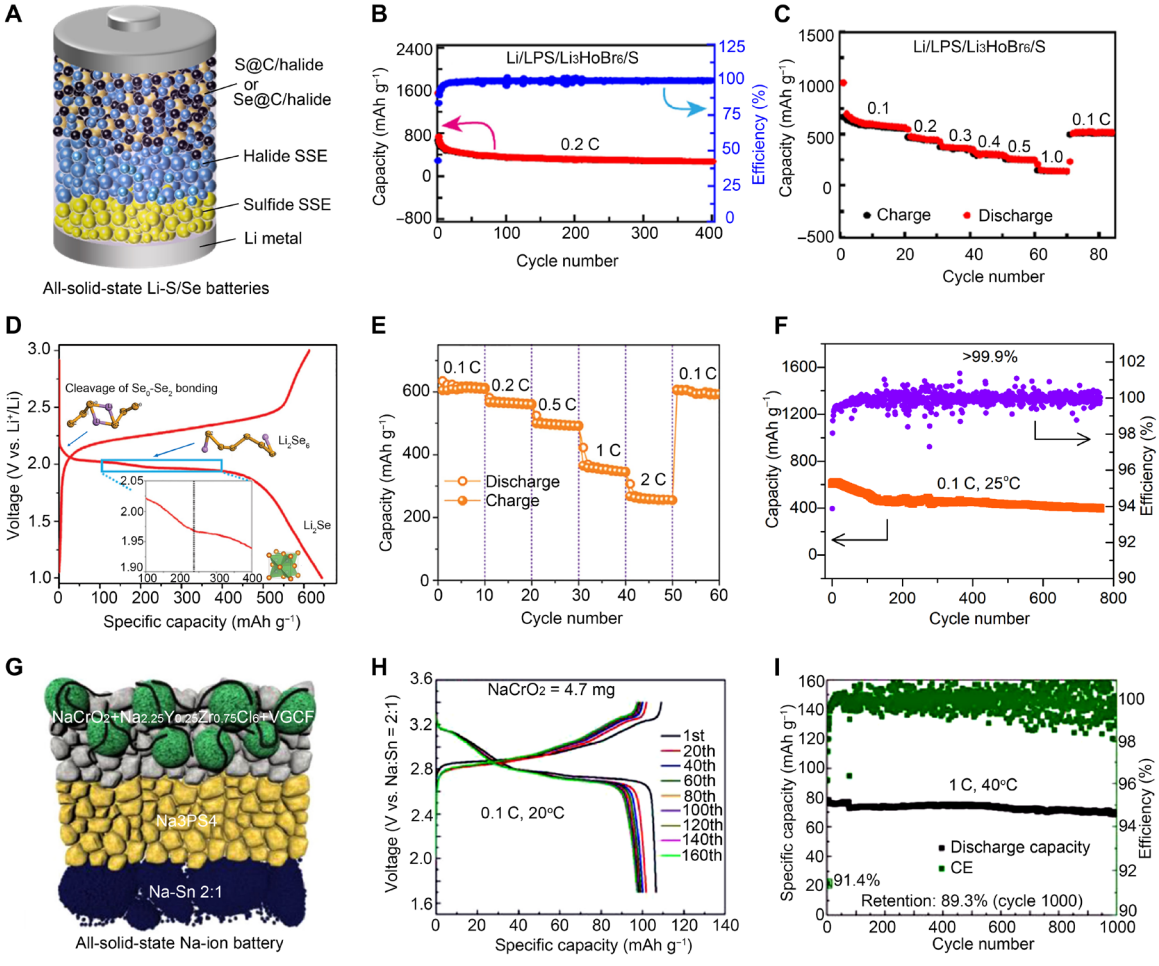

Fig. 6. Conversion-type all-solid-state lithium batteries and all-solid-state Na-ion batteries using halide SSEs. (**A**) Schematic illustration of all-solid-state Li-S and Li-Se batteries. (**B**) Cycling stability and (**C**) rate performance of the Li/Li_3PS4/Li_3HoBr_6/S battery at 60°C (1 C = 1675 mA g^{-1}). Adapted with permission from (*43*). Copyright 2021, ACS. (**D**) The typical discharge/charge profile of Se@C@Li_3HoCl_6 cathode at 50 mA g^{-1} with an enlarged discharge profile in the range of 1.90 to 2.05 V. (**E**) Rate performance and (**F**) cycling stability of Se@C@Li_3HoCl_6 cathode. Reproduced with permission from (*102*). Copyright 2022, Wiley. (**G**) Schematic illustration of all-solid-state Na-ion batteries with a configuration of $NaCrO_2$@$Na_{2.25}Y_{0.25}Zr_{0.75}Cl_6$@VGCF/$Na_3PS_4$/Na-Sn. (**H**) Charge-discharge curves of the all-solid-state Na-ion batteries at 0.1 C and 20°C. (**I**) Long-term cycling stability of all-solid-state Na-ion batteries at 1 C and 40°C. Reproduced with permission from (*56*) Copyright 2021, Springer Nature.

temperature and a wide electrochemical window (1.5 to 3.3 V versus Li^+/Li). When using it as the SSE, all-solid-state Li-S batteries exhibit a long cycling life of 400 cycles, high coulombic efficiency of close to 100% (Fig. 6B), and excellent rate performance (Fig. 6C), indicating the excellent chemical and electrochemical capability between halide SSEs and sulfur cathodes. Compared to sulfur (5×10^{-28} S cm^{-1}), selenium has a much higher electronic conductivity (1×10^{-3} S cm^{-1}) (*105*, *106*). Therefore, selenium chemistry has better kinetics than sulfur chemistry. Recently, our group demonstrated Li_3HoCl_6-based all-solid-state Li-Se batteries (*102*). Because of high-efficient charge transfer and excellent chemical and electrochemical compatibility, all-solid-state Li-Se batteries exhibit two distinctive plateaus in the discharge process (Fig. 6D). Regarding their rate performance, a high reversible capacity of 270 mAh g^{-1} is retained at 2 C. After reversing the current density to 0.1 C, a reversible capacity of 597 mAh g^{-1} is recovered (Fig. 6E). Moreover, this all-solid-state Li-Se battery shows stable cycling for 750 cycles and high coulombic efficiency greater than 99.9% (Fig. 6F). Solid-state Li-O_2 batteries that use Li_3InCl_6 as an interfacial modifier have also been demonstrated (*73*). Considering the catalytic activity of halogen chemistry in Li-O_2 and Li-S batteries (*73*, *107*, *108*), using halide SSEs as solid-state catalysts for developing solid-state Li-O_2 and Li-S batteries is a promising direction.

Along with the success of halide-based all-solid-state Li batteries, all-solid-state Na-ion batteries have also been demonstrated. For example, Meng *et al.* (*56*) reported a Na-ion conductor ($Na_{2.25}Y_{0.25}Zr_{0.75}Cl_6$) with an ionic conductivity of 0.066 mS cm^{-1} at ambient temperature, which is attributed to abundant Na vacancies and cooperative MCl_6 rotation. All-solid-state Na-ion batteries comprising a $NaCrO_2 + Na_{2.25}Y_{0.25}Zr_{0.75}Cl_6$ composite cathode, Na_3PS_4 electrolyte, and Na-Sn anode exhibit an exceptional first-cycle coulombic efficiency of 97.1% at room temperature can cycle over 1000 cycles with 89.3% capacity retention at 40°C (Fig. 6, G to I). These findings highlight the immense potential of halogen chemistry for developing all-solid-state Na-ion batteries (*56*). Foreseeably, all-solid-state Na-S, Na-O_2, and Na/Li-organic batteries can also be developed on the basis of halide SSEs (*109*, *110*).

Energy density evaluation and targets of halide ASSBs

Assuming that all the challenges at the material level are resolved, we further evaluated the feasibility of halide SSEs in practical solid-state pouch cells toward the energy density targets of 400 and 500 Wh kg^{-1}, respectively. Using typical $LiNi_{0.8}Mn_{0.1}Co_{0.1}O_2$ and Li metal as electrodes, the gravimetrical and volumetric energy densities of all-solid-state $LiNi_{0.8}Mn_{0.1}Co_{0.1}O_2$ (NMC811)/halide/Li pouch cells were analyzed (*111*–*113*). High-loading electrodes and ultrathin halide SSE membranes are crucial for achieving a high energy density (Fig. 7, A and B). It can be seen that 400 Wh kg^{-1} is attainable when 4 mAh cm^{-2} electrodes and 30-μm halide membranes are used in all-solid-state pouch cells (*2*). The corresponding volumetric energy density is 990 Wh liter^{-1}. Furthermore, the weight of each component in this 10 Ah is presented in Fig. 7C. Halide SSEs account for 28.2% of overall cost, which means that decreasing the cost of the halide SSEs can substantially reduce the entire cost of halide-based all-solid-state pouch cells.

All-solid-state Li-S chemistry using halide SSEs holds a great promise to attain a high energy density of 500 Wh kg^{-1} (*43*). Figure 7 (D and E) presents the gravimetrical and volumetric energy densities of

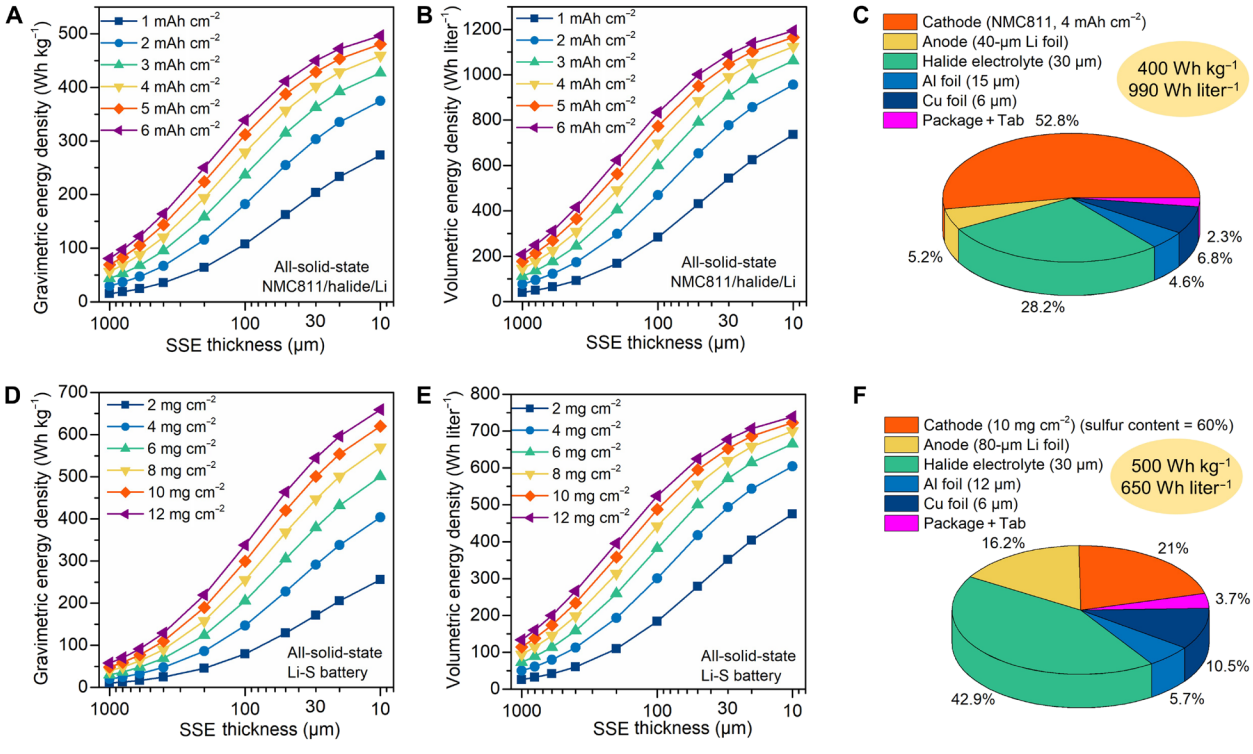

Fig. 7. Energy density evaluation of practical solid-state pouch cells based on halide SSEs. (**A** and **B**) Gravimetrical and volumetric energy density of all-solid-state NMC811/halide/Li batteries. (**C**) Component weight of a 10-Ah all-solid-state NMC811/halide/Li pouch cells. (**D** and **E**) Gravimetrical and volumetric energy density of halide-based all-solid-state Li-S batteries. (**F**) Component weight of 18.5-Ah halide-based all-solid-state Li-S pouch cells.

Table 1. Specific parameters required to achieve all-solid-state pouch cells with energy densities of 400 Wh kg^{-1} and 500 Wh kg^{-1}.

All-solid-state pouch cell system	Cathode materials ($LiNi_{0.8}Mn_{0.1}CoO_2$, 200 mAh g^{-1}; S_8, 1400 mAh g^{-1})					Li metal foil (3860 mAh g^{-1})	Halide electrolyte	Attainable energy density	
	Active material content (%)	Cathode loading (mg cm^{-2})	Areal capacity (mAh cm^{-2})	Thickness (μm)	Tap density (g cm^{-3})	Thickness (μm)	Thickness (μm)	Wh/liter	Wh/kg
Li-ion	85	27	4	80	3.4	40 μm	30	990	400
Li-S	60	10	8.4	70	1.4	80 μm	30	650	500

halide-based all-solid-state Li-S batteries. Similarly, a high-loading sulfur electrode with approximately 10 mg cm^{-2} (8.4 mAh cm^{-2}) should be attained to realize 500 Wh kg^{-1}. In addition, each component in an 18.5-Ah solid-state pouch cell is also broken down. The mass of the halide SSE accounts for 42.9% (Fig. 7F), indicating that reducing the cost of halide SSEs is critical for cost-effective all-solid-state Li-S pouch cells with an energy density of 500 Wh kg^{-1}. The corresponding volumetric energy density is 650 Wh liter^{-1}. It should be emphasized that the insufficient volumetric energy density of all-solid-state Li-S batteries can be further boosted by the rational design of sulfur composites with a high tap density (*114*), such as selenium-sulfur chemistry or transition metal sulfides (i.e., Co_8S_9) (*105*). The specific requirements for each component are specified in Table 1, acting as criteria for future development.

Conclusion and perspectives

In this Review, we first provide a fundamental understanding of SSEs using halogen chemistry and discuss their structural characteristics and design principles. Then, the current progress of halide SSEs is summarized according to their crystal structure. The feasibility of halide SSEs according to their cost and abundance is also discussed. Furthermore, various synthesis approaches are summarized, including mechanochemical synthesis, comelting, and wet-chemistry synthesis. It should be highlighted that both high-energy ball milling and wet-chemistry synthesis are promising synthesis methods for mass production. Now, the main issues hindering halide SSE development are moisture sensitivity and anode instability. Although these challenges have been somewhat alleviated by using ALD coatings, crystal structure tuning, and interfacial buffer layers, more efforts are still needed. In terms of their practical application, large format all-solid-state pouch cells using halide SSEs are simulated toward energy density targets of 400 Wh kg^{-1} (all-solid-state Li-ion batteries) and 500 Wh kg^{-1} (all-solid-state Li-S batteries). In addition, specific requirements of each component are listed to aid future endeavors.

Although remarkable progress has been made on halide SSEs, several crucial challenges have yet to be resolved. First, intensive fundamental studies are needed to gain a mechanistic understanding (e.g., structure-to-performance relationship) via advanced characterizations (e.g., in situ and ex situ) and theoretical calculation, which can help improve the ionic conductivity of halide SSEs to over 10 mS cm^{-1}. Some new mechanisms (i.e., paddle-wheel mechanism and multi-ion concerted migration) that govern ion transport of halide anion framework are worth studying. Second, developing fluoride-based halide SSEs with decent ionic conductivity and wide electrochemical windows is also desirable, as they can effectively enable high-capacity anodes (i.e., Li and Si anodes) and high-voltage cathodes (i.e., $LiNi_{0.5}Mn_{1.5}O_4$ and $LiCoPO_4$). Third, developing innovative, economically feasible, and environmentally benign synthesis routes is essential for the successful commercialization of halide SSEs. Fourth, along with the success of halide Li-ion superionic conductors, concerted efforts to develop other halide-based fast-ion conductors (i.e., Na-based) are also encouraged. Fifth, the moisture sensitivity of halide SSEs should be addressed so they can be easily handled in a dry room. Other than surface coatings and structural tuning that can ameliorate the poor air stability of halide SSEs, developing humidity-tolerant halide electrolytes with inherent moisture stability is a good direction. Sixth, the anode interfacial instability of halide SSEs should be overcome by designing a stable artificial solid electrolyte interphase with nitrides and synthesizing innovative halide SSEs that are highly chemical and electrochemical stable against anode materials. Seventh, lowering the cost of halide SSEs is a must for their large-scale application. This can be achieved using low-cost precursors, substituting precious elements with cheap elements, or developing cost-effective synthesis routes. Eighth, the dry-film method provides an effective way to explore engineering issues in all-solid-state pouch cells (*30*). The slurry coating process is compatible with current LIB roll-to-roll manufacturing, which has the advantages of high efficiency and low cost. Therefore, compatible solvents and binders, indispensable for the wet-chemistry slurry coating process, are highly desirable for mass production in the future. Last but not least, next-generation solid-state Li/Na batteries using sulfur, oxygen, and organic cathodes should be investigated on the basis of halide SSEs. Only targeting these advances and prospects will halide SSEs be able to make a smooth transition from fundamental study to practical application.

REFERENCES AND NOTES

1. J. Janek, W. G. Zeier, A solid future for battery development. *Nat. Energy* **1**, 16141 (2016).
2. Y.-G. Lee, S. Fujiki, C. Jung, N. Suzuki, N. Yashiro, R. Omoda, D.-S. Ko, T. Shiratsuchi, T. Sugimoto, S. Ryu, J. H. Ku, T. Watanabe, Y. Park, Y. Aihara, D. Im, I. T. Han, High-energy long-cycling all-solid-state lithium metal batteries enabled by silver–carbon composite anodes. *Nat. Energy* **5**, 299–308 (2020).
3. A. Manthiram, X. Yu, S. Wang, Lithium battery chemistries enabled by solid-state electrolytes. *Nat. Rev. Mater.* **2**, 16103 (2017).
4. L.-Z. Fan, H. He, C.-W. Nan, Tailoring inorganic–polymer composites for the mass production of solid-state batteries. *Nat. Rev. Mater.* **6**, 1003–1019 (2021).
5. X. Han, Y. Gong, K. Fu, X. He, G. T. Hitz, J. Dai, A. Pearse, B. Liu, H. Wang, G. Rubloff, Y. Mo, V. Thangadurai, E. D. Wachsman, L. Hu, Negating interfacial impedance in garnet-based solid-state Li metal batteries. *Nat. Mater.* **16**, 572–579 (2017).
6. K. Fu, Y. Gong, B. Liu, Y. Zhu, S. Xu, Y. Yao, W. Luo, C. Wang, S. D. Lacey, J. Dai, Y. Chen, Y. Mo, E. Wachsman, L. Hu, Toward garnet electrolyte–based Li metal batteries: An ultrathin, highly effective, artificial solid-state electrolyte/metallic Li interface. *Sci. Adv.* **3**, e1601659 (2017).
7. C. Wang, K. Fu, S. P. Kammampata, D. W. McOwen, A. J. Samson, L. Zhang, G. T. Hitz, A. M. Nolan, E. D. Wachsman, Y. Mo, V. Thangadurai, L. Hu, Garnet-type solid-state electrolytes: Materials, interfaces, and batteries. *Chem. Rev.* **120**, 4257–4300 (2020).

8. J. Liang, N. Chen, X. Li, X. Li, K. R. Adair, J. Li, C. Wang, C. Yu, M. N. Banis, L. Zhang, $Li_{10}Ge(P_{1-x}Sb_x)2S_{12}$ lithium-ion conductors with enhanced atmospheric stability. *Chem. Mater.* **32**, 2664–2672 (2020).
9. N. Kamaya, K. Homma, Y. Yamakawa, M. Hirayama, R. Kanno, M. Yonemura, T. Kamiyama, Y. Kato, S. Hama, K. Kawamoto, A. Mitsui, A lithium superionic conductor. *Nat. Mater.* **10**, 682–686 (2011).
10. Y. Kato, S. Hori, T. Saito, K. Suzuki, M. Hirayama, A. Mitsui, M. Yonemura, H. Iba, R. Kanno, High-power all-solid-state batteries using sulfide superionic conductors. *Nat. Energy* **1**, 16030 (2016).
11. Y. Yan, R.-S. Kühnel, A. Remhof, L. Duchêne, E. C. Reyes, D. Rentsch, Z. Łodziana, C. Battaglia, A lithium amide-borohydride solid-state electrolyte with lithium-ion conductivities comparable to liquid electrolytes. *Adv. Energy Mater.* **7**, 1700294 (2017).
12. M. Matsuo, S.-i. Orimo, Lithium fast-ionic conduction in complex hydrides: Review and prospects. *Adv. Energy Mater.* **1**, 161–172 (2011).
13. J. Liang, X. Li, K. R. Adair, X. Sun, Metal halide superionic conductors for all-solid-state batteries. *Acc. Chem. Res.* **54**, 1023–1033 (2021).
14. X. Li, J. Liang, X. Yang, K. R. Adair, C. Wang, F. Zhao, X. Sun, Progress and perspectives on halide lithium conductors for all-solid-state lithium batteries. *Energ. Environ. Sci.* **13**, 1429–1461 (2020).
15. L. Zhou, T.-T. Zuo, C. Y. Kwok, S. Y. Kim, A. Assoud, Q. Zhang, J. Janek, L. F. Nazar, High areal capacity, long cycle life 4 V ceramic all-solid-state Li-ion batteries enabled by chloride solid electrolytes. *Nat. Energy* **7**, 83–93 (2022).
16. T. Asano, A. Sakai, S. Ouchi, M. Sakaida, A. Miyazaki, S. Hasegawa, Solid halide electrolytes with high lithium-ion conductivity for application in 4 V class bulk-type all-solid-state batteries. *Adv. Mater.* **30**, 1803075 (2018).
17. S. Wang, Q. Bai, A. M. Nolan, Y. Liu, S. Gong, Q. Sun, Y. Mo, Lithium chlorides and bromides as promising solid-state chemistries for fast ion conductors with good electrochemical stability. *Angew. Chem. Int. Ed.* **58**, 8039–8043 (2019).
18. D. Ginnings, T. Phipps, Temperature-conductance curves of solid salts. III. Halides of lithium. *J. Am. Chem. Soc.* **52**, 1340–1345 (1930).
19. H. D. Lutz, K. Wussow, P. Kuske, Ionic conductivity, structural, IR and raman spectroscopic data of olivine, Sr_2PbO_4, and Na_2CuF_4 type lithium and sodium chlorides Li_2ZnCl_4 and Na_2MCl_4 (M = Mg, Ti, Cr, Mn, Co, Zn, Cd). *Z. Naturforsch. B* **42**, 1379–1386 (1987).
20. R. Kanno, Y. Takeda, M. Mori, O. Yamamoto, Ionic conductivity and structure of double chloride Li_2ZnCl_4 in the LiCl–$ZnCl_2$ system. *Chem. Lett.* **18**, 223–226 (1989).
21. A. Bohnsack, F. Stenzel, A. Zajonc, G. Balzer, M. S. Wickleder, G. Meyer, Ternary Halides of the A_3MX_6 type. VI. Ternary chlorides of the rare-earth elements with lithium, Li_3MCl_6 (M = Tb-Lu, Y, Sc): Synthesis, crystal structures, and ionic motion. *Z. Anorg. Allg. Chem.* **623**, 1067–1073 (1997).
22. C. Li, L. Gu, J. Maier, Enhancement of the Li conductivity in LiF by introducing glass/crystal interfaces. *Adv. Funct. Mater.* **22**, 1145–1149 (2012).
23. C. Li, L. Gu, X. Guo, D. Samuelis, K. Tang, J. Maier, Charge carrier accumulation in lithium fluoride thin films due to Li-ion absorption by titania (100) subsurface. *Nano Lett.* **12**, 1241–1246 (2012).
24. X. Li, J. Liang, N. Chen, J. Luo, K. R. Adair, C. Wang, M. N. Banis, T. K. Sham, L. Zhang, S. Zhao, Water-mediated synthesis of a superionic halide solid electrolyte. *Angew. Chem. Int. Ed.* **131**, 16579–16584 (2019).
25. X. Li, J. Liang, J. Luo, M. Norouzi Banis, C. Wang, W. Li, S. Deng, C. Yu, F. Zhao, Y. Hu, T.-K. Sham, L. Zhang, S. Zhao, S. Lu, H. Huang, R. Li, K. R. Adair, X. Sun, Air-stable Li_3InCl_6 electrolyte with high voltage compatibility for all-solid-state batteries. *Energ. Environ. Sci.* **12**, 2665–2671 (2019).
26. Z. Liu, S. Ma, J. Liu, S. Xiong, Y. Ma, H. Chen, High ionic conductivity achieved in $Li_3Y(Br_3Cl_3)$ mixed halide solid electrolyte via promoted diffusion pathways and enhanced grain boundary. *ACS Energy Lett.* **6**, 298–304 (2021).
27. B. Helm, R. Schlem, B. Wankmiller, A. Banik, A. Gautam, J. Ruhl, C. Li, M. R. Hansen, W. G. Zeier, Exploring aliovalent substitutions in the lithium halide superionic conductor $Li_{3-x}In_{1-x}Zr_xCl_6$ ($0 \le x \le 0.5$). *Chem. Mater.* **33**, 4773–4782 (2021).
28. T. Yu, J. Liang, L. Luo, L. Wang, F. Zhao, G. Xu, X. Bai, R. Yang, S. Zhao, J. Wang, J. Yu, X. Sun, Superionic fluorinated halide solid electrolytes for highly stable Li-metal in all-solid-state Li batteries. *Adv. Energy Mater.* **11**, 2101915 (2021).
29. Q. Shao, C. Yan, M. Gao, W. Du, J. Chen, Y. Yang, J. Gan, Z. Wu, W. Sun, Y. Jiang, Y. Liu, M. Gao, H. Pan, New insights into the effects of Zr substitution and carbon additive on $Li_{3-x}Er_{1-x}Zr_xCl_6$ Halide solid electrolytes. *ACS Appl. Mater. Interfaces* **14**, 8095–8105 (2022).
30. H. Kwak, S. Wang, J. Park, Y. Liu, K. T. Kim, Y. Choi, Y. Mo, Y. S. Jung, Emerging halide superionic conductors for all-solid-state batteries: Design, synthesis, and practical applications. *ACS Energy Lett.* **7**, 1776–1805 (2022).
31. M. Feinauer, H. Euchner, M. Fichtner, M. A. Reddy, Unlocking the potential of fluoride-based solid electrolytes for solid-state lithium batteries. *ACS Appl. Energy Mater.* **2**, 7196–7203 (2019).
32. J. Hu, K. Chen, C. Li, Nanostructured Li-rich fluoride coated by ionic liquid as high ion-conductivity solid electrolyte additive to suppress dendrite growth at Li metal anode. *ACS Appl. Mater. Interfaces* **10**, 34322–34331 (2018).
33. J. Hu, Z. Yao, K. Chen, C. Li, High-conductivity open framework fluorinated electrolyte bonded by solidified ionic liquid wires for solid-state Li metal batteries. *Energy Storage Mater.* **28**, 37–46 (2020).
34. J. Liang, X. Li, S. Wang, K. R. Adair, W. Li, Y. Zhao, C. Wang, Y. Hu, L. Zhang, S. Zhao, Site-occupation-tuned superionic Li_xScCl_{3+x}Halide solid electrolytes for all-solid-state batteries. *J. Am. Chem. Soc.* **142**, 7012–7022 (2020).
35. L. Zhou, C. Y. Kwok, A. Shyamsunder, Q. Zhang, X. Wu, L. F. Nazar, A new halospinel superionic conductor for high-voltage all solid state lithium batteries. *Energ. Environ. Sci.* **13**, 2056–2063 (2020).
36. S. Muy, J. Voss, R. Schlem, R. Koerver, S. J. Sedlmaier, F. Maglia, P. Lamp, W. G. Zeier, Y. Shao-Horn, High-throughput screening of solid-state Li-ion conductors using lattice-dynamics descriptors. *iScience* **16**, 270–282 (2019).
37. W. Ji, D. Zheng, X. Zhang, T. Ding, D. Qu, A kinetically stable anode interface for Li_3YCl_6-based all-solid-state lithium batteries. *J. Mater. Chem. A* **9**, 15012–15018 (2021).
38. H. Ito, K. Shitara, Y. Wang, K. Fujii, M. Yashima, Y. Goto, C. Moriyoshi, N. C. Rosero-Navarro, A. Miura, K. Tadanaga, Kinetically stabilized cation arrangement in Li_3YCl_6 superionic conductor during solid-state reaction. *Adv. Sci.* **8**, 2101413 (2021).
39. J. Liang, E. van der Maas, J. Luo, X. Li, N. Chen, K. R. Adair, W. Li, J. Li, Y. Hu, J. Liu, L. Zhang, S. Zhao, S. Lu, J. Wang, H. Huang, W. Zhao, S. Parnell, R. I. Smith, S. Ganapathy, M. Wagemaker, X. Sun, A series of ternary metal chloride superionic conductors for high-performance all-solid-state lithium batteries. *Adv. Energy Mater.* **12**, 2103921 (2022).
40. R. Schlem, A. Banik, S. Ohno, E. Suard, W. G. Zeier, Insights into the lithium sub-structure of superionic conductors Li_3YCl_6 and Li_3YBr_6. *Chem. Mater.* **33**, 327–337 (2021).
41. C. Yu, Y. Li, K. R. Adair, W. Li, K. Goubitz, Y. Zhao, M. J. Willans, M. A. Thijs, C. Wang, F. Zhao, Q. Sun, S. Deng, J. Liang, X. Li, R. Li, T.-K. Sham, H. Huang, S. Lu, S. Zhao, L. Zhang, L. van Eijck, Y. Huang, X. Sun, Tuning ionic conductivity and electrode compatibility of Li_3YBr_6 for high-performance all solid-state Li batteries. *Nano Energy* **77**, 105097 (2020).
42. S. Zhang, F. Zhao, S. Wang, J. Liang, J. Wang, C. Wang, H. Zhang, K. Adair, W. Li, M. Li, H. Duan, Y. Zhao, R. Yu, R. Li, H. Huang, L. Zhang, S. Zhao, S. Lu, T.-K. Sham, Y. Mo, X. Sun, Advanced high-voltage all-solid-state Li-ion batteries enabled by a dual-halogen solid electrolyte. *Adv. Energy Mater.* **11**, 2100836 (2021).
43. X. Shi, Z. Zeng, M. Sun, B. Huang, H. Zhang, W. Luo, Y. Huang, Y. Du, C. Yan, Fast Li-ion conductor of Li_3HoBr_6 for stable all-solid-state lithium–sulfur battery. *Nano Lett.* **21**, 9325–9331 (2021).
44. N. Adelstein, B. C. Wood, Role of dynamically frustrated bond disorder in a Li^+ superionic solid electrolyte. *Chem. Mater.* **28**, 7218–7231 (2016).
45. H. Kwak, D. Han, J. Lyoo, J. Park, S. H. Jung, Y. Han, G. Kwon, H. Kim, S.-T. Hong, K.-W. Nam, Y. S. Jung, New cost-effective halide solid electrolytes for all-solid-state batteries: Mechanochemically prepared Fe^{3+}-substituted Li_2ZrCl_6. *Adv. Energy Mater.* **11**, 2003190 (2021).
46. S. Y. Kim, K. Kaup, K.-H. Park, A. Assoud, L. Zhou, J. Liu, X. Wu, L. F. Nazar, Lithium ytterbium-based halide solid electrolytes for high voltage all-solid-state batteries. *ACS Mater. Lett.* **3**, 930–938 (2021).
47. K.-H. Park, K. Kaup, A. Assoud, Q. Zhang, X. Wu, L. F. Nazar, High-voltage superionic halide solid electrolytes for all-solid-state Li-ion batteries. *ACS Energy Lett.* **5**, 533–539 (2020).
48. J. Park, D. Han, H. Kwak, Y. Han, Y. J. Choi, K.-W. Nam, Y. S. Jung, Heat treatment protocol for modulating ionic conductivity via structural evolution of $Li_{3-x}Yb_{1-x}M_xCl_6$ (M = Hf^{4+}, Zr^{4+}) new halide superionic conductors for all-solid-state batteries. *Chem. Eng. J.* **425**, 130630 (2021).
49. G. Xu, L. Luo, J. Liang, S. Zhao, R. Yang, C. Wang, T. Yu, L. Wang, W. Xiao, J. Wang, J. Yu, X. Sun, Origin of high electrochemical stability of multi-metal chloride solid electrolytes for high energy all-solid-state lithium-ion batteries. *Nano Energy* **92**, 106674 (2021).
50. Z. Xu, X. Chen, K. Liu, R. Chen, X. Zeng, H. Zhu, Influence of anion charge on Li ion diffusion in a new solid-state electrolyte, Li_3LaI_6. *Chem. Mater.* **31**, 7425–7433 (2019).
51. R. Schlem, T. Bernges, C. Li, M. A. Kraft, N. Minafra, W. G. Zeier, Lattice dynamical approach for finding the lithium superionic conductor Li_3ErI_6. *ACS Appl. Energy Mater.* **3**, 3684–3691 (2020).
52. Y. Qie, S. Wang, S. Fu, H. Xie, Q. Sun, P. Jena, Yttrium–sodium halides as promising solid-state electrolytes with high ionic conductivity and stability for Na-ion batteries. *J. Phys. Chem. Lett.* **11**, 3376–3383 (2020).
53. D. Park, K. Kim, G. H. Chun, B. C. Wood, J. H. Shim, S. Yu, Materials design of sodium chloride solid electrolytes Na_3MCl_6 for all-solid-state sodium-ion batteries. *J. Mater. Chem. A* **9**, 23037–23045 (2021).
54. H. Kwak, J. Lyoo, J. Park, Y. Han, R. Asakura, A. Remhof, C. Battaglia, H. Kim, S.-T. Hong, Y. S. Jung, Na_2ZrCl_6 enabling highly stable 3 V all-solid-state Na-ion batteries. *Energy Storage Mater.* **37**, 47–54 (2021).
55. R. Schlem, A. Banik, M. Eckardt, M. Zobel, W. G. Zeier, $Na_{3-x}Er_{1-x}Zr_xCl6$—A halide-based fast sodium-ion conductor with vacancy-driven ionic transport. *ACS Appl. Energy Mater.* **3**, 10164–10173 (2020).
56. E. A. Wu, S. Banerjee, H. Tang, P. M. Richardson, J.-M. Doux, J. Qi, Z. Zhu, A. Grenier, Y. Li, E. Zhao, G. Deysher, E. Sebti, H. Nguyen, R. Stephens, G. Verbist, K. W. Chapman,

R. J. Clément, A. Banerjee, Y. S. Meng, S. P. Ong, A stable cathode-solid electrolyte composite for high-voltage, long-cycle-life solid-state sodium-ion batteries. *Nat. Commun.* **12**, 1256 (2021).
57. Y. Han, S. H. Jung, H. Kwak, S. Jun, H. H. Kwak, J. H. Lee, S.-T. Hong, Y. S. Jung, Single- or poly-crystalline Ni-rich layered cathode, sulfide or Halide solid electrolyte: Which will be the winners for all-solid-state batteries? *Adv. Energy Mater.* **11**, 2100126 (2021).
58. T. Oi, K. Miyauchi, Amorphous thin film ionic conductors of mLiF.nAlF$_3$. *Mater. Res. Bull.* **16**, 1281–1289 (1981).
59. Y. Liu, S. Wang, A. M. Nolan, C. Ling, Y. Mo, Tailoring the cation lattice for chloride lithium-ion conductors. *Adv. Energy Mater.* **10**, 2002356 (2020).
60. M. Gombotz, H. M. R. Wilkening, Fast Li ion dynamics in the mechanosynthesized nanostructured form of the solid electrolyte Li$_3$YBr$_6$. *ACS Sustain. Chem. Eng.* **9**, 743–755 (2021).
61. R. Yuan, Z. Zhe-Yi, Z. Qian, W. Da, Y. Jia, S. Si-Qi, Brief overview of microscopic physical image of ion transport in electrolytes. *Acta. Phys. Sin.* **69**, 226601 (2020).
62. Z. Zhang, H. Li, K. Kaup, L. Zhou, P.-N. Roy, L. F. Nazar, Targeting superionic conductivity by turning on anion rotation at room temperature in fast ion conductors. *Matter* **2**, 1667–1684 (2020).
63. Z. Zhang, L. F. Nazar, Exploiting the paddle-wheel mechanism for the design of fast ion conductors. *Nat. Rev. Mater.* **7**, 389–405 (2022).
64. X. He, Y. Zhu, Y. Mo, Origin of fast ion diffusion in super-ionic conductors. *Nat. Commun.* **8**, 15893 (2017).
65. D. Park, H. Park, Y. Lee, S.-O. Kim, H.-G. Jung, K. Y. Chung, J. H. Shim, S. Yu, Theoretical design of lithium chloride superionic conductors for all-solid-state high-voltage lithium-ion batteries. *ACS Appl. Mater. Interfaces* **12**, 34806–34814 (2020).
66. E. Umeshbabu, S. Maddukuri, Y. Hu, M. Fichtner, A. R. Munnangi, Influence of chloride ion substitution on lithium-ion conductivity and electrochemical stability in a dual-halogen solid-state electrolyte. *ACS Appl. Mater. Interfaces* **14**, 25448–25456 (2022).
67. S. Ohno, T. Bernges, J. Buchheim, M. Duchardt, A.-K. Hatz, M. A. Kraft, H. Kwak, A. L. Santhosha, Z. Liu, N. Minafra, F. Tsuji, A. Sakuda, R. Schlem, S. Xiong, Z. Zhang, P. Adelhelm, H. Chen, A. Hayashi, Y. S. Jung, B. V. Lotsch, B. Roling, N. M. Vargas-Barbosa, W. G. Zeier, How certain are the reported ionic conductivities of thiophosphate-based solid electrolytes? An interlaboratory study. *ACS Energy Lett.* **5**, 910–915 (2020).
68. R. Schlem, S. Muy, N. Prinz, A. Banik, Y. Shao-Horn, M. Zobel, W. G. Zeier, Mechanochemical synthesis: A tool to tune cation site disorder and ionic transport properties of Li$_3$MCl$_6$ (M = Y, Er) superionic conductors. *Adv. Energy Mater.* **10**, 1903719 (2020).
69. C. Wang, J. Liang, J. Luo, J. Liu, X. Li, F. Zhao, R. Li, H. Huang, S. Zhao, L. Zhang, J. Wang, X. Sun, A universal wet-chemistry synthesis of solid-state halide electrolytes for all-solid-state lithium-metal batteries. *Sci. Adv.* **7**, eabh1896 (2021).
70. E. Sebti, H. A. Evans, H. Chen, P. M. Richardson, K. M. White, R. Giovine, K. P. Koirala, Y. Xu, E. Gonzalez-Correa, C. Wang, C. M. Brown, A. K. Cheetham, P. Canepa, R. J. Clément, Stacking faults assist lithium-ion conduction in a halide-based superionic conductor. *J. Am. Chem. Soc.* **144**, 5795–5811 (2022).
71. K. Kim, D. Park, H.-G. Jung, K. Y. Chung, J. H. Shim, B. C. Wood, S. Yu, Material design strategy for halide solid electrolytes Li$_3$MX$_6$ (X = Cl, Br, and I) for all-solid-state high-voltage Li-ion batteries. *Chem. Mater.* **33**, 3669–3677 (2021).
72. G. Yang, X. Liang, S. Zheng, H. Chen, W. Zhang, S. Li, F. Pan, Li-rich channels as the material gene for facile lithium diffusion in halide solid electrolytes. *eScience* **2**, 79–86 (2022).
73. C. Zhao, J. Liang, X. Li, N. Holmes, C. Wang, J. Wang, F. Zhao, S. Li, Q. Sun, X. Yang, J. Liang, X. Lin, W. Li, R. Li, S. Zhao, H. Huang, L. Zhang, S. Lu, X. Sun, Halide-based solid-state electrolyte as an interfacial modifier for high performance solid-state Li–O$_2$ batteries. *Nano Energy* **75**, 105036 (2020).
74. F. D. Han, Y. Z. Zhu, X. F. He, Y. F. Mo, C. S. Wang, Electrochemical stability of Li$_{10}$GeP$_2$S$_{12}$ and Li$_7$La$_3$Zr$_2$O$_{12}$ solid electrolytes. *Adv. Energy Mater.* **6**, 1501590 (2016).
75. K. Wang, Q. Ren, Z. Gu, C. Duan, J. Wang, F. Zhu, Y. Fu, J. Hao, J. Zhu, L. He, C.-W. Wang, Y. Lu, J. Ma, C. Ma, A cost-effective and humidity-tolerant chloride solid electrolyte for lithium batteries. *Nat. Commun.* **12**, 4410 (2021).
76. Y. Zhu, Y. Mo, Materials design principles for air-stable lithium/sodium solid electrolytes. *Angew. Chem. Int. Ed.* **59**, 17472–17476 (2020).
77. S. Wang, X. Xu, C. Cui, C. Zeng, J. Liang, J. Fu, R. Zhang, T. Zhai, H. Li, Air sensitivity and degradation evolution of halide solid state electrolytes upon exposure. *Adv. Funct. Mater.* **32**, 2108805 (2022).
78. W. Li, J. Liang, M. Li, K. R. Adair, X. Li, Y. Hu, Q. Xiao, R. Feng, R. Li, L. Zhang, S. Lu, H. Huang, S. Zhao, T.-K. Sham, X. Sun, Unraveling the origin of moisture stability of Halide solid-state electrolytes by in situ and operando synchrotron x-ray analytical techniques. *Chem. Mater.* **32**, 7019–7027 (2020).
79. X. Li, J. Liang, K. R. Adair, J. Li, W. Li, F. Zhao, Y. Hu, T.-K. Sham, L. Zhang, S. Zhao, S. Lu, H. Huang, R. Li, N. Chen, X. Sun, Origin of superionic Li$_3$Y$_{1-x}$In$_x$Cl$_6$ halide solid electrolytes with high humidity tolerance. *Nano Lett.* **20**, 4384–4392 (2020).
80. A. Dańczak, L. Rycerz, Reinvestigation of the DyCl$_3$–LiCl binary system phase diagram. *J. Therm. Anal. Calorim.* **126**, 299–305 (2016).
81. R. Iwasaki, S. Hori, R. Kanno, T. Yajima, D. Hirai, Y. Kato, Z. Hiroi, Weak anisotropic lithium-ion conductivity in single crystals of Li$_{10}$GeP$_2$S$_{12}$. *Chem. Mater.* **31**, 3694–3699 (2019).
82. X. Shi, Z. Zeng, H. Zhang, B. Huang, M. Sun, H. H. Wong, Q. Lu, W. Luo, Y. Huang, Y. Du, C.-H. Yan, Gram-scale synthesis of nanosized Li$_3$HoBr$_6$ solid electrolyte for all-solid-state Li-Se battery. *Small Methods* **5**, 2101002 (2021).
83. M. Zhang, N. Garcia-Araez, A. L. Hector, Understanding and development of olivine LiCoPO$_4$ cathode materials for lithium-ion batteries. *J. Mater. Chem. A* **6**, 14483–14517 (2018).
84. G. Liang, V. K. Peterson, K. W. See, Z. Guo, W. K. Pang, Developing high-voltage spinel LiNi0.5 Mn1.5O4 cathodes for high-energy-density lithium-ion batteries: Current achievements and future prospects. *J. Mater. Chem. A* **8**, 15373–15398 (2020).
85. L. Riegger, R. Schlem, J. Sann, W. G. Zeier, J. Janek, Lithium-metal anode instability of the superionic Halide solid electrolytes and the implications for solid-state batteries. *Angew. Chem. Int. Ed.* **60**, 6718–6723 (2020).
86. Y. Zhang, C. Sun, Composite lithium protective layer formed in situ for stable lithium metal batteries. *ACS Appl. Mater. Interfaces* **13**, 12099–12105 (2021).
87. T. Koç, F. Marchini, G. Rousse, R. Dugas, J.-M. Tarascon, In search of the best solid electrolyte-layered oxide pairing for assembling practical all-solid-state batteries. *ACS Appl. Energy Mater.* **4**, 13575–13585 (2021).
88. F. Li, X. Cheng, L.-L. Lu, Y.-C. Yin, J.-D. Luo, G. Lu, Y.-F. Meng, H. Mo, T. Tian, J.-T. Yang, W. Wen, Z.-P. Liu, G. Zhang, C. Shang, H.-B. Yao, Stable all-solid-state lithium metal batteries enabled by machine learning simulation designed halide electrolytes. *Nano Lett.* **22**, 2461–2469 (2022).
89. C. Wang, T. Deng, X. Fan, M. Zheng, R. Yu, Q. Lu, H. Duan, H. Huang, C. Wang, X. Sun, Identifying soft breakdown in all-solid-state lithium battery. *Joule* 10.1016/j.joule.2022.05.020 (2022).
90. Y. Zhu, X. He, Y. Mo, Strategies based on nitride materials chemistry to stabilize Li metal anode. *Adv. Sci.* **4**, 1600517 (2017).
91. H. Maekawa, M. Matsuo, H. Takamura, M. Ando, Y. Noda, T. Karahashi, S.-i. Orimo, Halide-stabilized LiBH$_4$, a room-temperature lithium fast-ion conductor. *J. Am. Chem. Soc.* **131**, 894–895 (2009).
92. S. Kim, H. Oguchi, N. Toyama, T. Sato, S. Takagi, T. Otomo, D. Arunkumar, N. Kuwata, J. Kawamura, S.-i. Orimo, A complex hydride lithium superionic conductor for high-energy-density all-solid-state lithium metal batteries. *Nat. Commun.* **10**, 1081 (2019).
93. X. Lü, J. W. Howard, A. Chen, J. Zhu, S. Li, G. Wu, P. Dowden, H. Xu, Y. Zhao, Q. Jia, Antiperovskite Li$_3$OCl superionic conductor films for solid-state li-ion batteries. *Adv. Sci.* **3**, 1500359 (2016).
94. W. Xia, Y. Zhao, F. Zhao, K. Adair, R. Zhao, S. Li, R. Zou, Y. Zhao, X. Sun, Antiperovskite electrolytes for solid-state batteries. *Chem. Rev.* **122**, 3763–3819 (2022).
95. W. Liu, S. W. Lee, D. Lin, F. Shi, S. Wang, A. D. Sendek, Y. Cui, Enhancing ionic conductivity in composite polymer electrolytes with well-aligned ceramic nanowires. *Nat. Energy* **2**, 17035 (2017).
96. D. Zhou, D. Shanmukaraj, A. Tkacheva, M. Armand, G. Wang, Polymer electrolytes for lithium-based batteries: Advances and prospects. *Chem* **5**, 2326–2352 (2019).
97. D. H. S. Tan, Y.-T. Chen, H. Yang, W. Bao, B. Sreenarayanan, J.-M. Doux, W. Li, B. Lu, S.-Y. Ham, B. Sayahpour, J. Scharf, E. A. Wu, G. Deysher, H. E. Han, H. J. Hah, H. Jeong, J. B. Lee, Z. Chen, Y. S. Meng, Carbon-free high-loading silicon anodes enabled by sulfide solid electrolytes. *Science* **373**, 1494–1499 (2021).
98. F. Dou, L. Shi, G. Chen, D. Zhang, Silicon/carbon composite anode materials for lithium-ion batteries. *Electrochem. Energ. Rev.* **2**, 149–198 (2019).
99. H. Pan, M. Zhang, Z. Cheng, H. Jiang, J. Yang, P. Wang, P. He, H. Zhou, Carbon-free and binder-free Li-Al alloy anode enabling an all-solid-state Li-S battery with high energy and stability. *Sci. Adv.* **8**, eabn4372 (2022).
100. S. Y. Han, C. Lee, J. A. Lewis, D. Yeh, Y. Liu, H.-W. Lee, M. T. McDowell, Stress evolution during cycling of alloy-anode solid-state batteries. *Joule* **5**, 2450–2465 (2021).
101. S. Luo, Z. Wang, X. Li, X. Liu, H. Wang, W. Ma, L. Zhang, L. Zhu, X. Zhang, Growth of lithium-indium dendrites in all-solid-state lithium-based batteries with sulfide electrolytes. *Nat. Commun.* **12**, 6968 (2021).
102. X. Li, J. Liang, J. T. Kim, J. Fu, H. Duan, N. Chen, R. Li, S. Zhao, J. Wang, H. Huang, X. Sun, Highly stable halide-electrolyte-based all-solid-state Li–Se batteries. *Adv. Mater.* **34**, 2200856 (2022).
103. C. Wang, K. Adair, X. Sun, All-solid-state lithium metal batteries with sulfide electrolytes: Understanding interfacial ion and electron transport. *Acc. Mater. Res.* **3**, 21–32 (2022).
104. H. Chen, C. Wang, W. Dong, W. Lu, Z. Du, L. Chen, Monodispersed sulfur nanoparticles for lithium–sulfur batteries with theoretical performance. *Nano Lett.* **15**, 798–802 (2015).
105. X. Li, J. Liang, J. Luo, C. Wang, X. Li, Q. Sun, R. Li, L. Zhang, R. Yang, S. Lu, High-performance Li–SeS$_x$ all-solid-state lithium batteries. *Adv. Mater.* **31**, 1808100 (2019).
106. X. Li, J. Liang, X. Li, C. Wang, J. Luo, R. Li, X. Sun, High-performance all-solid-state Li–Se batteries induced by sulfide electrolytes. *Energ. Environ. Sci.* **11**, 2828–2832 (2018).
107. X. Bi, J. Li, M. Dahbi, J. Alami, K. Amine, J. Lu, Understanding the role of lithium iodide in lithium–oxygen batteries. *Adv. Mater.* **34**, 2106148 (2022).

108. H. Wan, B. Zhang, S. Liu, J. Zhang, X. Yao, C. Wang, Understanding LiI-LiBr catalyst activity for solid state Li2S/S reactions in an all-solid-state lithium battery. *Nano Lett.* **21**, 8488–8494 (2021).
109. Y. Lu, J. Chen, Prospects of organic electrode materials for practical lithium batteries. *Nat. Rev. Chem.* **4**, 127–142 (2020).
110. F. Hao, X. Chi, Y. Liang, Y. Zhang, R. Xu, H. Guo, T. Terlier, H. Dong, K. Zhao, J. Lou, Y. Yao, Taming active material-solid electrolyte interfaces with organic cathode for all-solid-state batteries. *Joule* **3**, 1349–1359 (2019).
111. C. Wang, J. Liang, Y. Zhao, M. Zheng, X. Li, X. Sun, All-solid-state lithium batteries enabled by sulfide electrolytes: From fundamental research to practical engineering design. *Energ. Environ. Sci.* **14**, 2577–2619 (2021).
112. J. Wu, L. Yuan, W. Zhang, Z. Li, X. Xie, Y. Huang, Reducing the thickness of solid-state electrolyte membranes for high-energy lithium batteries. *Energ. Environ. Sci.* **14**, 12–36 (2021).
113. L. Liu, J. Xu, S. Wang, F. Wu, H. Li, L. Chen, Practical evaluation of energy densities for sulfide solid-state batteries. *eTransportation* **1**, 100010 (2019).
114. Y.-T. Liu, S. Liu, G.-R. Li, X.-P. Gao, Strategy of enhancing the volumetric energy density for lithium–sulfur batteries. *Adv. Mater.* **33**, 2003955 (2021).
115. R. D. Shannon, Revised effective ionic radii and systematic studies of interatomic distances in halides and chalcogenides. *Acta Crystallogr. A* **32**, 751–767 (1976).

Acknowledgments
Funding: This work was supported by the Natural Sciences and Engineering Research Council of Canada (NSERC), the Canada Research Chair Program (CRC), the Canada Foundation for Innovation (CFI), the Ontario Research Fund, and the University of Western Ontario. C.W. acknowledges the Banting Postdoctoral Fellowship (BPF-180162). **Author contributions:** C.W. conceived the Review and wrote the content. J.L. contributed to the discussion of the content. J.T.K. and X.S. edited and reviewed the article before submission. **Competing interests:** The authors declare that they have no competing interests. **Data and materials availability:** All data needed to evaluate the conclusions in the paper are present in the paper.

Submitted 11 May 2022
Accepted 22 July 2022
Published 7 September 2022
10.1126/sciadv.adc9516

Prospects of halide-based all-solid-state batteries: From material design to practical application

Changhong WangJianwen LiangJung Tae KimXueliang Sun

Sci. Adv., 8 (36), eadc9516. • DOI: 10.1126/sciadv.adc9516